Acta Crystallographica Section D
Biological Crystallography
ISSN 0907-4449

Exploring binding sites other than the catalytic core in the crystal structure of the catalytic domain of MKP-4

Dae Gwin Jeong,[a]‡ Tae Sung Yoon,[a]‡ Suk-Kyeong Jung,[a] Byoung Cheol Park,[a] Hwangseo Park,[b] Seong Eon Ryu[a,c]* and Seung Jun Kim[a]*

[a]Medical Proteomics Research Center, Korea Research Institute of Bioscience and Biotechnology, 52 Eoeun-Dong, Yuseong-Gu, Daejeon 305-333, Republic of Korea, [b]Department of Bioscience and Biotechnology, Sejong University, 98 Kunja-Dong, Kwangjin-Ku, Seoul 143-147, Republic of Korea, and [c]Department of Bio Engineering, Hanyang University, Seongdong-Gu, Seoul 133-791, Republic of Korea

‡ These authors contributed equally to this work.

Correspondence e-mail: ryuse@hanyang.ac.kr, ksj@kribb.re.kr

Received 18 February 2010
Accepted 19 October 2010

PDB Reference: catalytic domain of MKP-4, 3lj8.

Map kinase phosphatase 4 (MKP-4), which has been implicated in signalling pathways that negatively regulate glucose uptake, belongs to the dual-specificity phosphatase (DUSP) family. An inherent property of MKPs is an ability to undergo structural rearrangement, transitioning from a partially active to a fully active conformation. Here, a 2.7 Å resolution crystal structure of the catalytic domain of MKP-4 (MKP-4C) is presented. It was determined that the MKP-4C structure seriously deviates from canonical conformations of DUSPs and this characteristic feature results in significant gaps between the catalytic core and several surrounding loops which are unique compared with other MKP counterparts that adopt an active conformation. Using virtual library screening, it was found that inhibitors bind to MKP-4C with high affinity near these gaps. Inhibitors that target other binding sites instead of the active site can be utilized to prevent transition to a fully active conformation. Compounds that are able to make contacts with these sites in MKP-4 would not only provide a beneficial increase in affinity but may also permit greater specificity relative to other protein tyrosine phosphatases.

1. Introduction

The reciprocal phosphorylating and dephosphorylating activities of protein tyrosine kinases and protein tyrosine phosphatases (PTPs; EC 3.1.3.48), respectively, are hallmarks of cellular signal transduction (Tonks, 2006). Of the 107 members of the PTP superfamily identified in the human genome, 61 are classified as dual-specific phosphatases (DUSPs; Alonso *et al.*, 2004) based on analysis of their catalytic domains. DUSPs have dual dephosphorylation activity at the activation loop (-pT-*X*-pY-) of mitogen-activated protein kinases (MAPKs) and thereby regulate all aspects of signal transduction pathways, including growth and differentiation, cell motility, metabolism, apoptosis and immune responses. The mitogen-activated protein kinase phosphatase (MKP) family of DUSPs has 11 members, all of which contain a MAPK-binding domain in the N-terminal region in addition to a catalytic domain (Farooq & Zhou, 2004). The MKP-family member MKP-4 appears to have broad specificity towards three MAPK substrates: extracellular signal-regulated kinase (ERK), c-Jun N-terminal kinase (JNK) and p38 (Muda *et al.*, 1997). MKP-4 is expressed in insulin-sensitive tissues and overexpression of MKP-4 is observed in obese insulin-resistant rodent models (Xu *et al.*, 2003). Moreover, up-regulation of MKP-4 in

Table 1
Data-collection and refinement statistics.

Values in parentheses are for the highest resolution shell.

Data collection	
Wavelength (Å)	1.0
Space group	$P3_221$
Unit-cell parameters (Å, °)	$a = b = 91.93$, $c = 56.61$, $\alpha = \beta = 90$, $\gamma = 120$
Resolution (Å)	50–2.70 (2.85–2.70)
Total reflections	44183
Unique reflections	7730
Completeness (%)	98.4 (98.5)
Multiplicity	5.7 (6.0)
$R_{\rm merge}$† (%)	3.2 (22.8)
$\langle I/\sigma(I)\rangle$	14.7 (3.4)
Refinement	
No. of reflections	7646
No. of atoms	1175
$R_{\rm cryst}/R_{\rm free}$	0.245/0.304
R.m.s. deviations from ideal geometry	
Bond distances (Å)	0.008
Bond angles (°)	1.58
Impropers (°)	1.10
Dihedrals (°)	22.9
Average B factors (Å^2)	
Main-chain atoms	65.3
Side-chain atoms	68.4

† $R_{\rm merge} = \sum_{hkl}\sum_i |I_i(hkl) - \langle I(hkl)\rangle| / \sum_{hkl}\sum_i I_i(hkl)$, where $I_i(hkl)$ is the intensity of the ith measurement of an equivalent reflection with indices hkl.

adipocytes inhibits glucose uptake, suggesting that MKP-4 may be a promising therapeutic target for the treatment of diabetes or metabolic syndrome. Despite substantial effort, the search for clinically effective inhibitors of individual PTPs has rarely been successful because of difficulties in the achievement of sufficient selectivity and/or bio-availability. These problems arise because of the shallow pocket and highly charged nature of the active sites of PTPs.

Here, we report the crystal structure of the catalytic domain of MKP-4 (MKP-4C) at 2.7 Å resolution. We found that the structure of the active-site region of MKP-4 significantly deviates from the canonical conformation of PTPs, providing an explanation for the low catalytic activity of MKP-4 in the absence of cognate substrates (Camps *et al.*, 1998). We also compared the structures of MKP-4 and other MKPs, identifying unique structural characteristics of MKP-4 that can be exploited as additional binding sites for inhibitors, and further confirmed these findings by virtual library screening. The structural features identified here provide a useful tool for exploring the selectivity and efficacy of MKP-4 inhibition and thereby may contribute to the development of therapeutically useful agents for the treatment of diabetes.

2. Materials and methods

2.1. Expression and purification

MKP-4C (residues 201–351; accession code NM001395) was cloned from human kidney cDNA (Clontech) and subcloned into a modified pET28a vector (Novagen) containing a maltose-binding protein (MBP; Roche) and an rTEV protease site between *Xba*I and *Nde*I restriction sites. The MBP-MKP-4C fusion protein, containing an additional His_6 tag at the N-terminus, was expressed in *Escherichia coli* BL21 (DE3) strain. Cells were induced for 16 h with 0.5 m*M* isopropyl β-D-1-thiogalactopyranoside and then grown at 291 K. Cells were harvested and sonicated in lysis buffer consisting of 50 m*M* Tris–HCl pH 7.5, 500 m*M* NaCl, 1 m*M* phenylmethylsulfonyl fluoride, 0.04%(*v*/*v*) 2-mercaptoethanol and 5%(*v*/*v*) glycerol. The His_6-tagged MBP-MKP-4C fusion protein was then purified by nickel-affinity chromatography, cleaved by digestion with rTEV protease and reapplied onto the nickel-affinity column to separate cleaved from uncleaved fusion protein. The unbound fraction containing the MKP-4C protein was further purified by Q-Sepharose ion-exchange chromatography and Sephacryl S-100 gel-filtration chromatography. The purified protein was dialyzed against a buffer consisting of 20 m*M* Tris–HCl pH 8.5, 0.2 *M* NaCl, 2 m*M* DTT and 5% glycerol and concentrated to 20 mg ml^{-1} for use in crystallization.

2.2. Crystallization and data collection

Crystallization was performed at 291 K using the hanging-drop vapour-diffusion method. Initial trials were carried out using commercial screening kits (Hampton Research). The best crystals were grown by mixing 1.8 µl protein solution (20 mg ml^{-1}) with an equal volume of reservoir solution consisting of 10% ethanol, 1.3 *M* NaCl and 0.2 *M* magnesium sulfate. After 3–4 d, MKP-4C crystals had grown to their full size. X-ray diffraction data were collected on beamline 5A at the Photon Factory (Tsukuba, Japan) using an ADSC Quantum 315 detector. The crystal in the droplet was transferred into a cryosolution consisting of the mother liquor supplemented with 20%(*v*/*v*) glycerol and was immediately flash-frozen in a nitrogen-gas stream at 93 K. The crystal diffracted to 2.7 Å resolution and belonged to space group $P3_221$. The collected diffraction data were processed and scaled with *MOSFLM* (Leslie, 1999) and *SCALA* (Collaborative Computational Project, Number 4, 1994). The statistics of data collection and refinement are shown in Table 1.

2.3. Structure solution and refinement

Initial phases were obtained by the molecular-replacement method using MKP-5 (PDB code 1zzw) as a search model (Jeong *et al.*, 2006). The program *Phaser* (McCoy *et al.*, 2005) placed one monomer in the asymmetric unit of the crystal. The structure was refined using the program *CNS* (Brünger *et al.*, 1998). A randomly selected subset (5%) of the data was set aside for calculation of $R_{\rm free}$. Refinement included an overall anisotropic B-factor and bulk-solvent correction. Rounds of refinement were performed with manual rebuilding using the program *O* (Jones *et al.*, 1991). Figures were prepared using *PyMOL* (http://www.pymol.org).

2.4. Virtual screening

A docking library for MKP-4C comprising about 85 000 compounds was constructed from the latest version of the

chemical database distributed by InterBioScreen (http://www.ibscreen.com), which contains approximately 30 000 natural and 320 000 synthetic compounds. The selection was based on drug-like filters that accept only those compounds with the physicochemical properties of potential drug candidates (Lipinski *et al.*, 1997) and which lack reactive functional groups. Three-dimensional atomic coordinates for all compounds included in the docking library were generated using *CORINA* v.3.1, followed by the assignment of Gasteiger–Marsilli atomic charges (Gasteiger & Marsili, 1980). We used *AutoDock* v.3.05 (Morris *et al.*, 1998) in the virtual screening of MKP-4C inhibitors. AMBER force-field parameters were assigned for calculation of the van der Waals interactions and the internal energy of a ligand as implemented in the *AutoDock* program. Docking simulations with *AutoDock* were then carried out with no constraints in the active site of MKP-4C to score and rank the compounds in the docking library according to their calculated binding affinities. The original scoring function of *AutoDock* v.3.05 proposed by Morris *et al.* (1998) was used in this virtual screening with the default parameters for all energy terms. The calculated grid maps were of dimensions of 61 × 61 × 61 points with a spacing of 0.375 Å, yielding a receptor model that includes atoms within 11.4 Å of the grid centre. In the docking simulations, we used the implicit solvation model with the distance-dependent dielectric constant proposed by Mehler & Solmajer (1991).

The three-dimensional coordinates of MKP-4C determined from X-ray crystallographic analysis were used as the receptor model in the virtual screening with docking simulations. After removing the solvent molecules, H atoms were added to each protein atom. Special attention was paid to assigning the protonation states of the ionizable Asp, Glu, His and Lys residues. The side chains of Asp and Glu residues were assumed to be neutral if one of their carboxylate O atoms pointed towards a hydrogen-bond-accepting group, including the backbone aminocarbonyl O atom, with a distance within 3.5 Å, which is a generally accepted distance limit for a hydrogen bond of moderate strength. Similarly, the lysine side chains were assumed to be protonated unless the NZ atom was in the proximity of a hydrogen-bond-donating group. The same procedure was also applied to determine the protonation states of ND and NE atoms of His residues. On the other hand, all amino and carboxylic acid groups in the ligands were assumed to be ionized.

2.5. *In vitro* enzymatic assay

Compounds were tested in inhibition assays using the same protocol as described in our previous studies (Park *et al.*, 2008). All compounds purchased from InterBioScreen were evaluated for their *in vitro* inhibitory activity against recombinant human MKP-4C. Assays were performed using 6,8-difluoro-4-methylumbelliferyl phosphate (DIFMUP) as a substrate at 298 K for 5 min in 20 m*M* Tris–HCl pH 8.0 and 5 m*M* DTT in the presence or absence of inhibitor (90 µ*M*) dissolved in dimethylsulfoxide. After adding purified MKP-4C (0.3 µ*M*) and DIFMUP (5 µ*M*), the reactions were allowed to proceed for 20 min at room temperature and were stopped by adding sodium orthovanadate (1 m*M*). The fluorescence intensity was measured (355 nm excitation and 460 nm emission) using a plate reader. IC_{50} values were determined

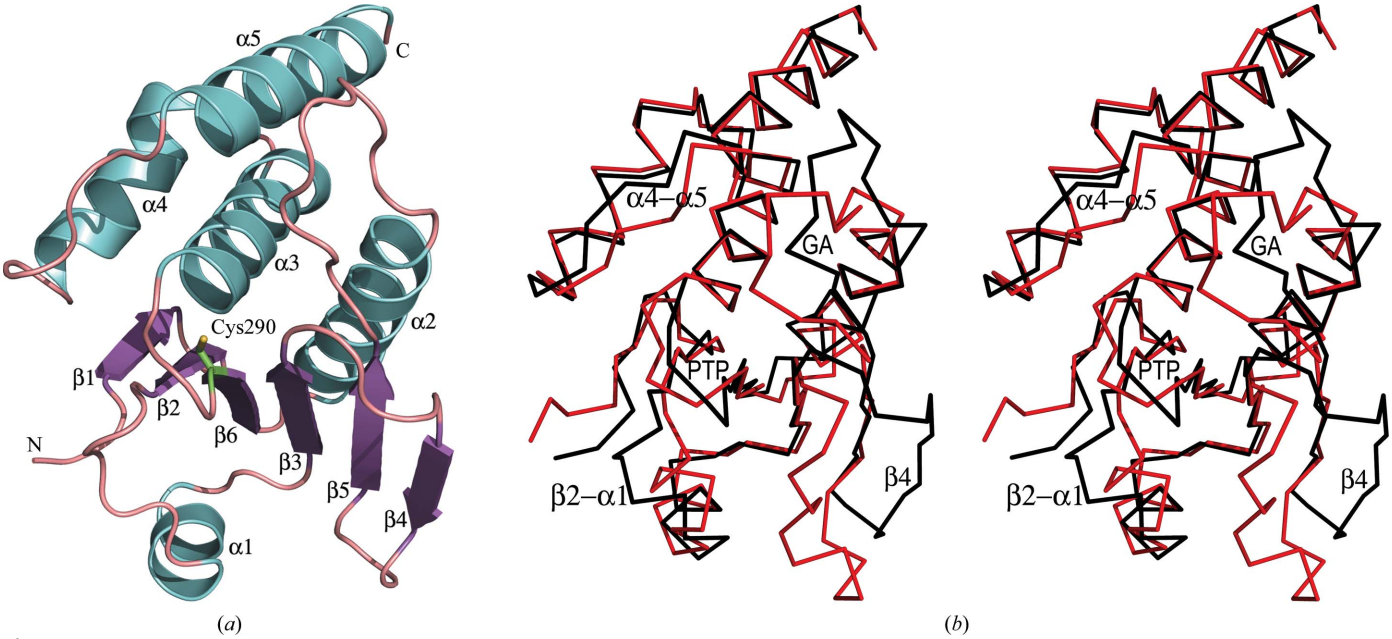

(*a*) (*b*)

Figure 1
Crystal structure of MKP-4C. (*a*) Ribbon representation of the catalytic domain of MKP-4. Secondary-structural boundaries are α1, 222–228; α2, 268–282; α3, 295–309; α4, 311–323; α5, 331–346; β1, 205–208; β2, 211–214; β3, 232–237; β4, 243–246; β5, 251–255; β6, 285–289. (*b*) Comparison of C^{α} traces. The C^{α} trace of MKP-4C (black) is superimposed on that of MKP-5C (red). Superposition was performed with the program *O* (Jones *et al.*, 1991) using a criterion of less than 3.8 Å for more than three consecutive C^{α} atoms. The regions that significantly deviate are labelled on the drawing. PTP, PTP-loop; GA, general acid loop.

Table 2
IC_{50} values of the compounds against MKP-4C with their ranking in virtual screening.

Compound	IC_{50} (μM)	Ranking
1	8.8	31
2	13.9	87
3	28.7	5
4	26.6	48
5	55.4	11

directly from regression curves constructed using at least five different concentrations of each inhibitor.

3. Results and discussion

3.1. Overall structure of MKP-4C

The crystal structure of MKP-4C (residues 202–348) was solved by molecular replacement at a resolution of 2.7 Å. One molecule of MKP-4C was found in the asymmetric unit and no indications of oligomeric interactions were found in the crystal. The final R_{cryst} and R_{free} values were 0.245 and 0.304, respectively. The model was validated using *PROCHECK* (Laskowski *et al.*, 1993) and *MolProbity* (Chen *et al.*, 2010). A Ramachandran plot showed that 87.8 and 10.7% of all residues were within the most favoured and additionally allowed regions, respectively. There were no residues in the disallowed regions and the all-atom contacts clash score was 13.6 (94th percentile). Overall, the geometry and electron-density map were of good quality. The structure of MKP-4C is formed by a central six-stranded β-sheet with four helices (α2–α5) on one face and one (α1) on the other (Fig. 1*a*). The active site of MKP-4C consists of a PTP-loop (His-Cys290-*X*-*X*-Gly-*X*-*X*-Arg-Ser/Thr, where *X* is any amino acid) and Asp259, which acts as a general acid. The canonically active conformation of cysteine-based PTPs can be defined by the low-pK_a-value (5.0–5.5) thiol group of the active-site cysteine, the main-chain amide atoms of the PTP-loop, which are directed toward the inside of the PTP-loop embracing the active-site cysteine, and the presence of aspartate as a general acid in the proximity of the PTP-loop (Zhang, 2002).

In an alignment of the structure of MKP-4C with that of MKP-5C (PDB code 1zzw; Jeong *et al.*, 2006), the human MKP family member with the highest resolution structure generated to date, 118 of 147 MKP-4C residues could be superimposed with a root-mean-square deviation of 1.2 Å. There were several important structural differences between the two enzymes (Fig. 1*b*). Firstly, the region of MKP-4C corresponding to the MKP-5C β3–β4 loop, which is located above the β-sheet and interacts extensively with helix α1 and the PTP-loop, forms β-strand β4. Secondly, the PTP-loop of MKP-4C significantly deviates in structure from that of MKP-5C (Fig. 2). Although the side chain of Cys290 is positioned at the bottom of the PTP-loop, the orientation of the thiol group is not ideal for efficient enzyme catalysis. In addition, the general acid loop containing Asp259 in MKP-4C is ∼3 Å away from the corresponding region in MKP-5C. The α4–α5 and β2–α1 loops are also moved away from the catalytic core in MKP4, resulting in the creation of long deep clefts. Overall, the crystal contacts in MKP-4C appear to be less extensive than those in MKP-5C (solvent content of crystals: MKP-4C, 70%; MKP-5C, 47%). These structural deviations are thought to reflect the well known substrate-induced activation properties of MKP-4 (Camps *et al.*, 1998). The isolated MKP-4 catalytic domain displays very low catalytic activity. However, MKP-4 has been shown to exhibit full catalytic activity upon binding to MAPK using the N-terminal MKB domain. Indeed, several MAPKs have been shown to dramatically enhance the catalytic activity of MKP-4 by binding to this domain

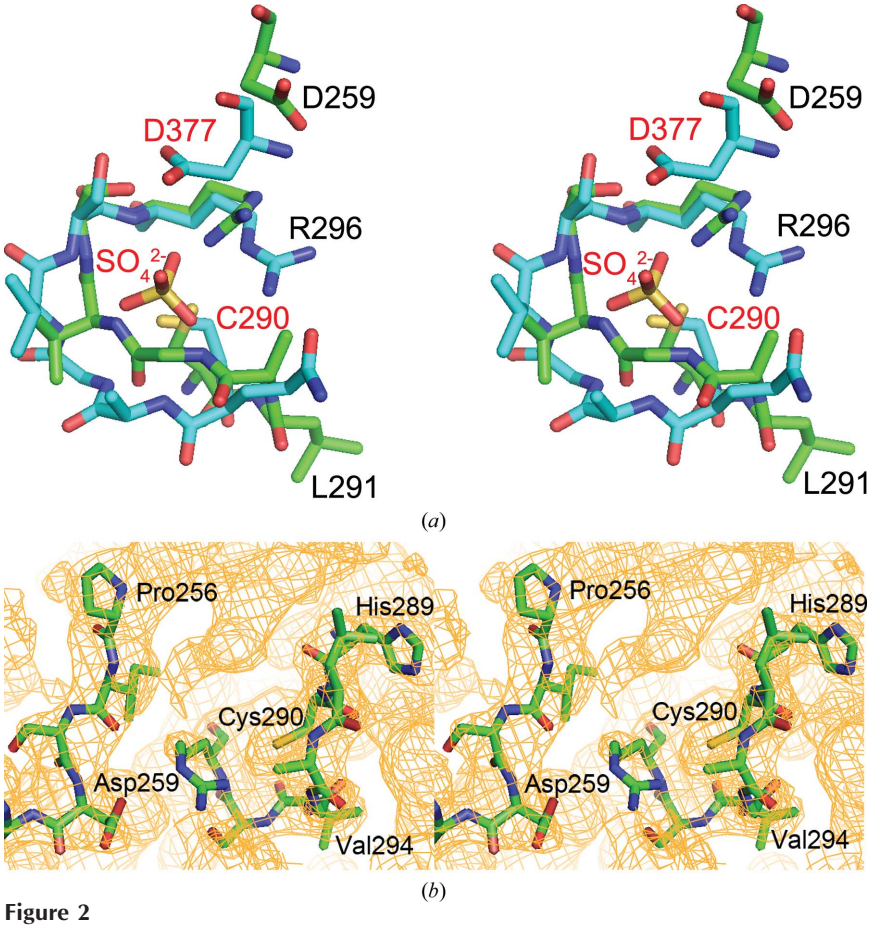

Figure 2
Active site. (*a*) Comparison of active sites. The active sites of MKP-4C (green) and MKP-5C (cyan) in complex with sulfate ion are superimposed and presented as stick models. MKP-4C residues are labelled in black, whereas MKP-5C residues are labelled in red. (*b*) The $2F_o - F_c$ map for MKP-4C was generated with the final model, omitting residues less than 3.5 Å distant from Cys290. The map is contoured at the 1σ level. Residues in the PTP-loop (289–296) are superimposed on the map.

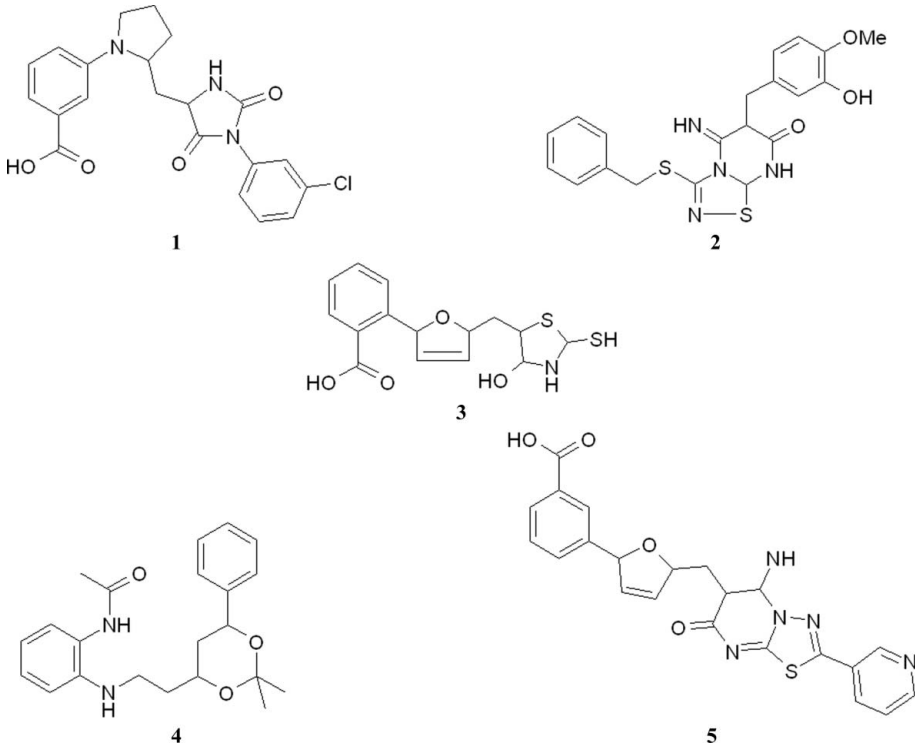

Figure 3
Chemical structures of MKP-4 inhibitors.

(Camps *et al.*, 1998). Substrate binding is thought to trigger catalytically important residues to adopt the canonical conformation of PTP for catalysis. Compared with MKP-5, which shows robust activity irrespective of MAPK binding, the catalytic efficiency of MKP-4C is ∼100-fold lower than that of MKP-5C in the absence of MKB (Jeong *et al.*, 2006). These results support the idea that MKP-4 is an MKP that follows a substrate-induced activation mechanism, both structurally and biochemically; movements of loops surrounding the PTP-loop upon cognate substrate binding would fill the gap between the outer rim of the PTP-loop and its surrounding loops in MKP-4C (Fig. 1*b*).

3.2. Virtual ligand library screening

The presence of the prominent gap between the PTP-loop and its surrounding loops in the MKP-4C structure led us to perform virtual ligand screening in order to identify small molecules that could bind to these regions away from the catalytic core. Of the 85 000 compounds subjected to virtual screening with docking simulations, 100 top-scoring compounds were selected as virtual hits and their inhibitory activities towards MKP4-C were evaluated. Among these, five compounds revealed high potency (more than 70% inhibition at 90 μ*M*) and were selected for determination of IC_{50} values. The chemical structures and inhibitory activities of these compounds are shown in Fig. 3 and Table 2. Compound **1** (3-{2-[1-(3-chlorophenyl)-2,5-dioxoimidazolidin-4-ylmethyl]-pyrrolidin-1-yl}benzoic acid) displayed the greatest inhibitory activity towards MKP-4C. To obtain some energetic and structural insight into the inhibitory mechanisms of the newly identified inhibitors, their binding modes around the active sites of MKP-C were investigated with the *AutoDock* program using the procedure described above. It should be noted that only the lowest-energy binding mode of an inhibitor is discussed in this paper, although the docking simulations indicated the possibility of several binding modes for each inhibitor. The modelled structure of the MKP-4C–**1** complex shows that compound **1** resides in the active site of MKP-4C, with the carboxylate group of compound **1** in contact with the main-chain amide atoms of the PTP-loop (Fig. 4 and Supplementary Fig. 1[1]). However, another factor is also likely to contribute to binding because the remaining portion of compound **1** makes many van der Waals contacts with residues from the α4–α5 loop and the PTP-loop. Unlike the MKP-4C–**1** complex, compound **2** {3-benzylsulfanyl-6-(3-hydroxy-4-methoxybenzyl)-5-imino-5,6,8,8a-tetrahydro-[1,2,4]thiadiazolo-[4,5-*a*]pyrimidin-7-one} makes no direct contact with residues interior to the PTP-loop. Modelling suggests that compound **2** binding occurs at a cleft surrounded by the general acid loop, the α4–α5 loop and the upper part of helix α3. The thiadiazolopyrimidine group of compound **2** is buried deep in the cleft and makes many good contacts with residues of MKP-4C, contacts that appear to make a major contribution to the inhibitory activity. The MKP-4C residues participating in binding to compound **2** are Asp259, His260, Gln307, Asn330, Phe331 and Phe333. As with compound **2**, compounds **3** {2-[5-(4-hydroxy-2-mercaptothiazolidin-5-ylmethyl)-2,5-dihydrofuran-2-yl]benzoic acid}, **4** (*N*-{2-[2-(2,2-dimethyl-6-phenyl-[1,3]dioxin-4-yl)ethylamino]-phenyl}acetamide) and **5** [3-(5-imino-7-oxo-2-pyridin-3-yl-6,7-dihydro-5*H*-[1,3,4]thiadiazolo-[3,2-*a*]pyrimidin-6-ylmethyl)-2,5-dihydrofuran-2-yl)benzoic acid] do not contact residues interior to the PTP-loop. The binding pattern of compounds **3**–**5** differs from that of compound **2** in that these compounds are sandwiched between the α4–α5 loop and the PTP-loop. A portion of each compound is buried deep within a cleft between the α4–α5 loop and the PTP-loop and makes extensive van der Waals contacts with hydrophobic residues, notably Val294, Val298, Val302, Tyr317, Ile327 and Pro329. Except for compound **1**, the binding sites lie between the PTP-loop and the loops surrounding the PTP-loop. The binding of compounds **2**–**5** would block movement of the loops into the active conformation, which could explain their

[1] Supplementary material has been deposited in the IUCr electronic archive (Reference: KW5021). Services for accessing this material are described at the back of the journal.

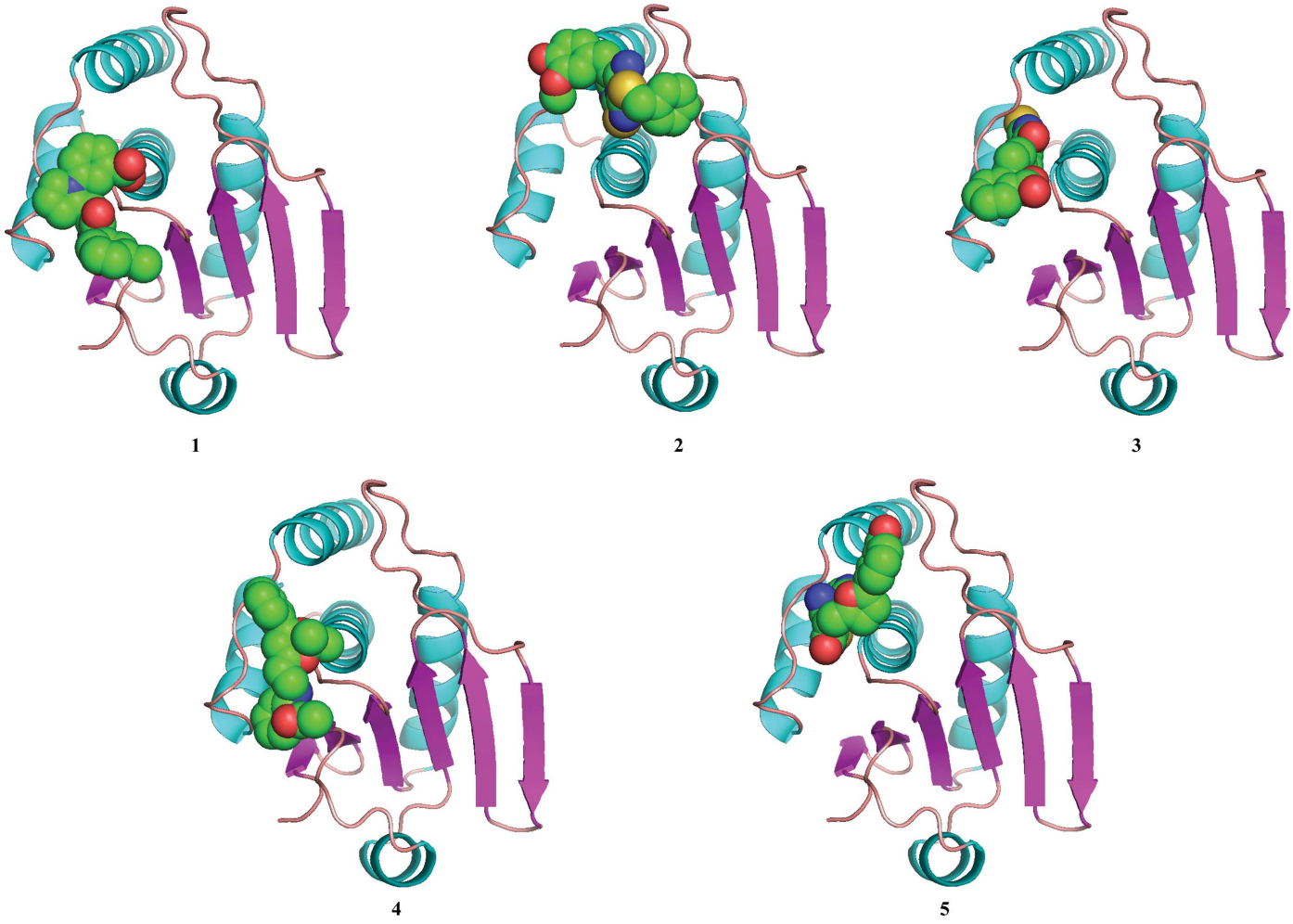

Figure 4
A comparison of the binding pattern of MKP-4C with compounds **1**–**5**. MKP-4C is represented as a ribbon, whereas compounds **1**–**5** are depicted as van der Waals surfaces. C, N, O and S atoms are coloured grey, blue, red and yellow, respectively.

inhibitory activities. Drugs targeted to these areas might prevent the rearrangement of either the α4–α5 loop or the general acid loop upon substrate binding because the compounds would occupy the region involved in conformational transition during induction of activation (Jeong *et al.*, 2006) (Fig. 1*b*). Given the conserved structural and biochemical characteristics of the MKP members that follow an induced-activation mechanism (Stewart *et al.*, 1999; Farooq *et al.*, 2001), the targeting of clefts formed by the PTP-loop and surrounding loops could be exploited to improve both the efficacy and specificity of inhibition.

4. Conclusions

The crucial role of PTPs in regulating signal transduction, highlighted by recent examples of human diseases caused by the disruption of PTP function, has made it clear that human PTPs may be viable targets in new drug-development efforts. However, 103 cysteine-directed PTPs have active sites in common in humans, profoundly complicating the task of developing selective compounds. Indeed, there are many examples of failed drug-discovery projects that have targeted PTPs (Zhang & Zhang, 2007; Blaskovich, 2009). Recently, a unique allosteric site was found in the PTP1B structure and this is now being exploited to develop a drug to prevent diabetes (Wiesmann *et al.*, 2004). Similarly, the unique interaction of particular compounds with MKP-4 may provide a template for the design of MKP-4-specific therapeutic agents. The residues identified here that participate in the binding of these compounds are not highly conserved compared with the residues of the active site (see Supplementary Fig. 2), increasing the prospects of developing isoform-specific drugs. An additional challenge in traditional drug-development efforts has been the hydrophilic character of the active site of PTPs. The clefts found in MKP4-C are much less hydrophilic than the active site and may thus serve as a good target for the rational design of drugs to prevent changes to the active conformation of MKP-4. Such drugs might ultimately prove to be effective against insulin-independent diabetes mellitus; however, further studies to improve affinity are required if such compounds are to play a therapeutic role *in vivo*.

The atomic coordinates and structural parameters of the final structure have been deposited in the PDB under code 3lj8.

The authors thank the staff of the Photon Factory BL5A and Pohang Accelerator Laboratory beamline 4A for help in collecting diffraction data. This work was supported by a grant from the Korea Research Institute of Bioscience and Biotechnology Research Initiative Program and a grant from the World Class Institute Program of the National Research Foundation of Korea, funded by the Ministry of Education, Science and Technology.

References

Alonso, A., Sasin, J., Bottini, N., Friedberg, I., Friedberg, I., Osterman, A., Godzik, A., Hunter, T., Dixon, J. & Mustelin, T. (2004). *Cell*, **117**, 699–711.

Blaskovich, M. A. T. (2009). *Curr. Med. Chem.* **16**, 2095–2176.

Brünger, A. T., Adams, P. D., Clore, G. M., DeLano, W. L., Gros, P., Grosse-Kunstleve, R. W., Jiang, J.-S., Kuszewski, J., Nilges, M., Pannu, N. S., Read, R. J., Rice, L. M., Simonson, T. & Warren, G. L. (1998). *Acta Cryst.* D**54**, 905–921.

Camps, M., Nichols, A., Gillieron, C., Antonsson, B., Muda, M., Chabert, C., Boschert, U. & Arkinstall, S. (1998). *Science*, **280**, 1262–1265.

Chen, V. B., Arendall, W. B., Headd, J. J., Keedy, D. A., Immormino, R. M., Kapral, G. J., Murray, L. W., Richardson, J. S. & Richardson, D. C. (2010). *Acta Cryst.* D**66**, 12–21.

Collaborative Computational Project, Number 4 (1994). *Acta Cryst.* D**50**, 760–763.

Farooq, A., Chaturvedi, G., Mujtaba, S., Plotnikova, O., Zeng, L., Dhalluin, C., Ashton, R. & Zhou, M. M. (2001). *Mol. Cell*, **7**, 387–399.

Farooq, A. & Zhou, M. M. (2004). *Cell. Signal.* **16**, 767–779.

Gasteiger, J. & Marsili, M. (1980). *Tetrahedron*, **36**, 3219–3228.

Jeong, D. G., Yoon, T.-S., Kim, J. H., Shim, M. Y., Jung, S.-K., Son, J. H., Ryu, S. E. & Kim, S. J. (2006). *J. Mol. Biol.* **360**, 946–955.

Jones, T. A., Zou, J.-Y., Cowan, S. W. & Kjeldgaard, M. (1991). *Acta Cryst.* A**47**, 110–119.

Laskowski, R. A., MacArthur, M. W., Moss, D. S. & Thornton, J. M. (1993). *J. Appl. Cryst.* **26**, 283–291.

Leslie, A. G. W. (1999). *Acta Cryst.* D**55**, 1696–1702.

Lipinski, C. A., Lombardo, F., Dominy, B. W. & Feeney, P. (1997). *Adv. Drug Deliv. Rev.* **23**, 3–25.

McCoy, A. J., Grosse-Kunstleve, R. W., Storoni, L. C. & Read, R. J. (2005). *Acta Cryst.* D**61**, 458–464.

Mehler, E. L. & Solmajer, T. (1991). *Protein Eng.* **4**, 903–910.

Morris, G. M., Goodsell, D. S., Halliday, R. S., Huey, R., Hart, W. E., Belew, R. K. & Olson, A. J. (1998). *J. Comput. Chem.* **19**, 1639–1662.

Muda, M., Boschert, U., Smith, A., Antonsson, B., Gillieron, C., Chabert, C., Camps, M., Martinou, I., Ashworth, A. & Arkinstall, S. (1997). *J. Biol. Chem.* **272**, 5141–5151.

Park, H., Jung, S.-K., Jeong, D. K., Ryu, S. E. & Kim, S. J. (2008). *Bioorg. Med. Chem. Lett.* **18**, 2250–2255.

Stewart, A. E., Dowd, S., Keyse, S. M. & McDonald, N. Q. (1999). *Nature Struct. Biol.* **6**, 174–181.

Tonks, N. K. (2006). *Nature Rev. Mol. Cell Biol.* **7**, 833–846.

Wiesmann, C., Barr, K. J., Kung, J., Zhu, J., Erlanson, D. A., Shen, W., Fahr, B. J., Zhong, M., Taylor, L., Randal, M., McDowell, R. S. & Hansen, S. K. (2004). *Nature Struct. Mol. Biol.* **11**, 730–737.

Xu, H., Dembski, M., Yang, Q., Moriarty, A., Tayber, O., Chen, H., Kapeller, R. & Tartaglia, L. A. (2003). *J. Biol. Chem.* **278**, 30187–30192.

Zhang, S. & Zhang, Z.-Y. (2007). *Drug Discov. Today*, **12**, 373–381.

Zhang, Z.-Y. (2002). *Annu. Rev. Pharmacol. Toxicol.* **42**, 209–234.